Journal of Power Sources 242 (2013) 195–201

Contents lists available at SciVerse ScienceDirect

Journal of Power Sources

journal homepage: www.elsevier.com/locate/jpowsour

# Experimental investigation on a polymer electrolyte membrane fuel cell (PEMFC) parallel flow field design with external two-valve regulation on cathode channels

Shijie Tong, John C. Bachman, Anthony Santamaria, Jae Wan Park*

*Department of Mechanical and Aerospace Engineering, University of California, Davis, CA 95616, USA*

## HIGHLIGHT

- A novel parallel flow field design with external two-valve regulations.
- Design surpasses performance of parallel and interdigitated at high current density.
- The net performance enhancement is 10.9% at peak power density.

## ARTICLE INFO

*Article history:*
Received 11 December 2012
Received in revised form
10 April 2013
Accepted 9 May 2013
Available online 17 May 2013

*Keywords:*
PEM fuel cell
Cross flow
Two valve regulation
Parallel flow field

## ABSTRACT

Parallel/interdigitated/serpentine flow field PEM fuel cells have similar performance under low overvoltage operation. At higher overvoltage, interdigitated/serpentine flow field performance may exceed parallel flow field designs due to better water removal and more uniform reactant distribution by convective reactant flow in the GDL under land area, i.e. cross flow. However, serpentine flow field design suffers from high pumping losses and the risk of local flooding at channel U-bends. Additionally, interdigitated flow field designs may have higher local flooding risk in the inlet channels and relatively large pumping requirement at low current densities. In this study, a novel parallel flow field design with external two-valve regulation on the cathode was presented. Two valves introduced continuous pressure differences to two separate manifolds in the cathode that induce cross flow across the land areas. Moreover, both valves remained partially open to maintain a good water removal from flow channels. Comparative test results showed the proposed design surpasses performance of both parallel and interdigitated flow field design at operation current density of 0.7 A $cm^{-2}$ or higher. The performance enhancement is 10.9% at peak power density point (0.387 W $cm^{-2}$ @ 0.99 A $cm^{-2}$) compared to parallel flow field taking into account pumping losses.



## 1. Introduction

Proton exchange membrane fuel cells (PEMFCs) require proper hydration of the membrane electrode assembly (MEA). Liquid water concentration at cathode catalyst layer (CL) and gas diffusion layer (GDL), if not timely removed, will cause local flooding issues that result in performance degradation. A flow field design with good water management is able to effectively transport reactant gas through the fuel cell channels/GDL to force water out of CL and GDL porous media to channels [1]. Parallel flow field, interdigitated flow field and serpentine flow field are three typical flow field designs. Their differences in flow field geometry have little influence on the overall PEMFC performance at low overvoltage operation. While at high overvoltage operation, serpentine/interdigitated flow fields exhibit higher performance than parallel flow fields [2–5]. This is due to the high pressure flow which possesses nature pressure gradients (serpentine flow field) or forced pressure gradients (interdigitated flow field with baffles) between channels that induces cross flow at land areas, resulting in better water removal [1,6,7] and more uniform reactant distribution [8] at the cost of higher pumping power.

The distribution of water concentration in a PEMFC is closely associated with flow field geometry. For parallel flow fields, cross flow is minimal due to lack of a significant pressure gradient under the land area, where local flooding has a high chance of occurring [9,10] as illustrated in Fig. 1(a). For interdigitated flow field designs, water can have higher concentration in the downstream portions of the inlet channels due to blocked channel outlet as illustrated in Fig. 1(b) [2,3,10–12]. Serpentine flow field U-bends have higher

* Corresponding author.
*E-mail address:* jwpark@ucdavis.edu (J.W. Park).

0378-7753/$ – see front matter © 2013 Elsevier B.V. All rights reserved.
http://dx.doi.org/10.1016/j.jpowsour.2013.05.018

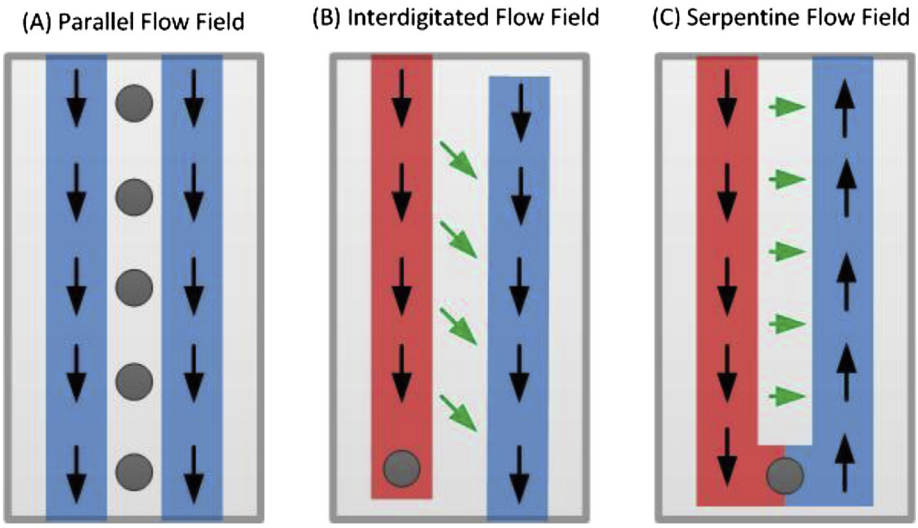


**Fig. 1.** Schematic of areas with high possibility for local flooding (grey dot) in (a) parallel, (b) interdigitated, and (c) serpentine flow fields.

water concentration because the surface area is larger so is the adhesive forces of accumulated water as illustrated in Fig. 1(c) [2,6,10,12–17].

In order to achieve better overall performance of PEMFCs, many novel flow patterns have been proposed and studied using approaches such as neutron radiography/tomography [11,18–20], 1D/2D current density mapping [13,21,22] and CFD simulation [3,6–8,14]. Suresh et al. [15] proposed a novel serpentine flow field design implementing enhanced cross flow to improve water removal at U-bend locations. Reshetenko et al. [23] experimentally validated the fact that over potential distributions along the flow field channels become more homogeneous with an increasing back pressure. Bachman et al. [9] proposed a novel parallel flow field with back pressure design by fabricating a parallel flow field PEMFC with two manifolds and increasing one manifold back pressure via a valve and pressure chamber. This design observed performance enhancement in polarization curve test at low operation potential region compared to parallel flow field design for different stoichiometry. A review of bipolar plates with various flow field designs was presented by Li et al. [24].

Inspired by Bachman's design [9], a parallel flow field design with two external valves regulation is presented in this study. The design expectations in this project are to create a new flow pattern which has a more uniform pressure difference at land area that

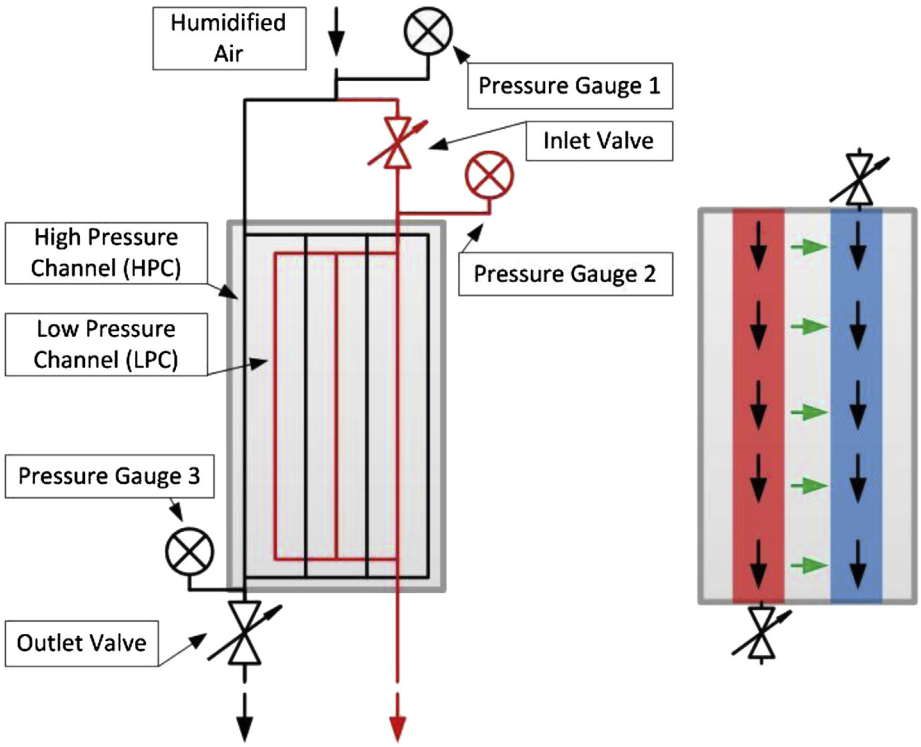


**Fig. 2.** Schematic of PEM fuel cell two-valve regulation experimental setup. Left: a PEM fuel cell was machined with two manifolds: HPCs (black) and LPCs (red). Pressure regulating valves was applied at HPC inlet and LPC outlet. Pressure gauges were utilized at the gas humidifier outlet, LPC inlet, and HPC outlet; Right: the two valves regulated parallel flow field design makes the HPCs (red) have higher-average pressure than LPCs (blue), which induces cross flow over the land area as indicated by green arrows in the figure. (For interpretation of the references to colour in this figure legend, the reader is referred to the web version of this article.)

induces cross flow along the channel and thus improves the overall performance of a PEMFC. At the same time, this flow field design will not lead to significant pumping losses or large concentration gradients as observed in serpentine/interdigitated flow field design. A detailed introduction to the proposed flow field design and experimental procedures is presented in Section 2. Fuel cell test results are presented and discussed in Section 3.

## 2. Experimental setup

### 2.1. Two-valve regulated parallel flow field design

As presented in Fig. 2 left, the fuel cell provided two manifolds for the cathode using two external valves: 4 channels were designated as high pressure channels (HPCs) with an outlet valve attached to the HPCs gas outlet; The 3 channels in between 4 HPCs were designated as low pressure channels (LPCs) with an inlet valve attached to the shared gas inlet. By adjusting the inlet and outlet valve to half open, HPCs had an enhanced back pressure at outlet, LPCs had pressure drop at the inlet. As illustrated in Fig. 2 right, pressure differences distribute along the channel land areas from inlets to outlets, inducing cross flow from HPCs to LPCs. Because the two valves allows for all 7 channels inlet and outlet to be open, only a part of reactant gas will travel through land area and the rest remains as parallel flow. This design is an intermediate flow field condition between parallel and interdigitated flow field.

### 2.2. Test setup

A PEM fuel cell was fabricated in order achieve the proposed flow field design. The fuel cell used two aluminium plates and brass electrical contacts for bipolar plates, 7 channels were machined into the plates. The flow channels are 20 cm long, 1 mm wide, 1 mm deep, and have 1 mm wide land areas. The gas diffusion layer (GDL) material used was SGL 10BC carbon; the membrane electrolyte was a Nafion 112 membrane with platinum loading of 0.4 mg per $cm^2$ on both sides. The active area of the fuel cell was approximately: 20.3 cm $\times$ 1.5 cm $=$ 30.45 $cm^2$. Based on the proposed flow field design, on the cathode, 4 HPCs shared a same gas inlet/outlet as one manifold; 3 LPCs shared a same gas inlet/outlet as the other manifold.

An Arbin fuel cell test station (FCTS) was used in the experiment. The cell was mounted vertically to a stand with its inlet on the top and outlet on the bottom. As shown in Fig. 3, pressure gauge 1 was used to measure the pump pressure of reactant gas that was sent by FCTS. The reactant gas on the cathode (humidified air) was split into two streams. One stream flew through the HPCs, a cylindrical chamber and an outlet valve (the cylindrical chamber and the outlet valve formed a back pressure regulator that maintained the desired back pressure as well as held the drained water); the other stream flow through an inlet valve to the LPCs. Pressure at the LPCs inlet was measured by pressure gauge 2; pressure at the HPCs outlet was measured by pressure gauge 3.

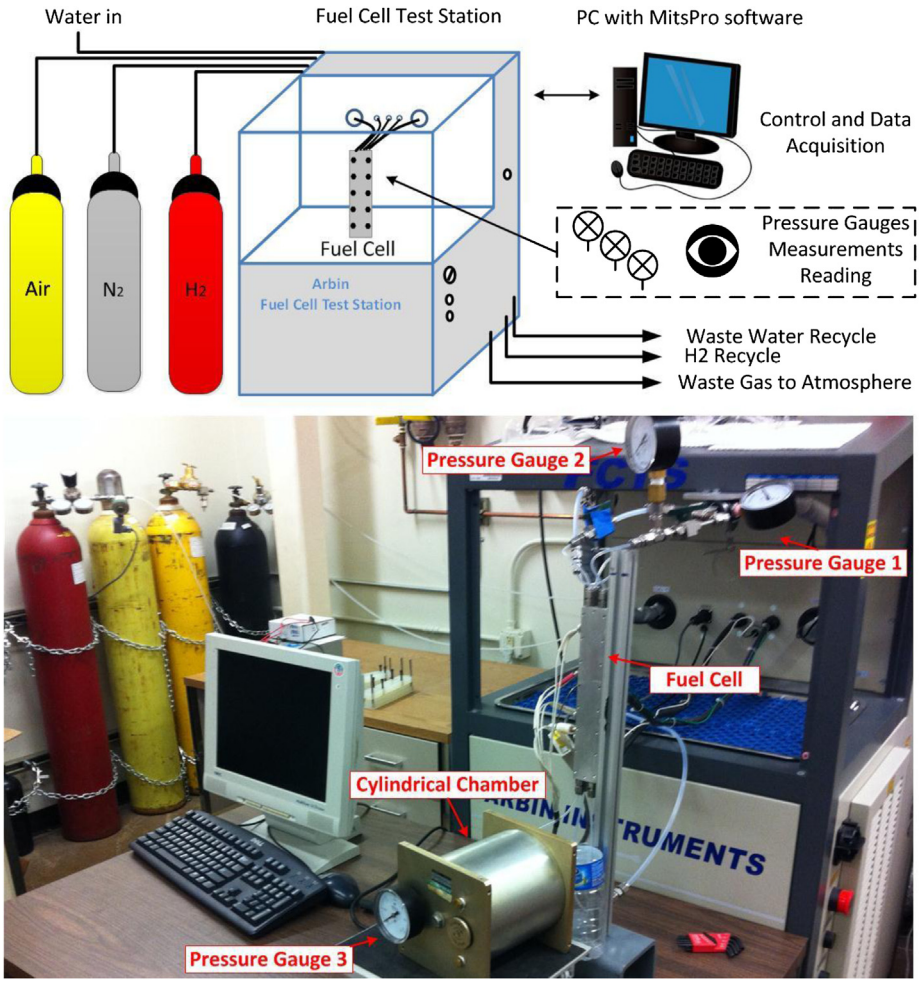


**Fig. 3.** Fuel cell test station setup.

### 2.3. Comparative test cases

The experimental setup was capable of testing various flow field designs through external valves adjustment of the fuel cell. Open valves allow for parallel flow, closed valves allow for interdigitated flow. As illustrated in Fig. 4, eight different flow fields were tested for comparison in this study:

- Case 1, Inlet valve open, outlet valve open (parallel flow filed);
- Case 2, Inlet valve open, outlet valve half open case;
- Case 3, Inlet valve open, outlet valve close case;
- Case 4, Inlet valve half open, outlet valve open case;
- Case 5, Inlet valve half open, outlet valve half open case (proposed flow field);
- Case 6, Inlet valve half open, outlet valve close case;
- Case 7, Inlet valve close, outlet valve half open case;
- Case 8, Inlet valve close, outlet valve close case (interdigitated flow field).

For conciseness, all the test cases will be referred as Case 1–8 in the rest of this paper. It was assumed that the pressure differences between HPCs and LPCs would induce cross flow. Gas flow under the land area will enhance water removal and achieve better reactant gas distribution along the MEA, which can enhance cell performance. Another assumption is that the closing of inlet/outlet valve will result in high water concentration at closed inlet/outlet which can reduce the cell performance. Case 5, as the proposed flow field design in this study, was expected to have the maximum induced cross flow and the minimum water concentration area compared to the rest of the cases.

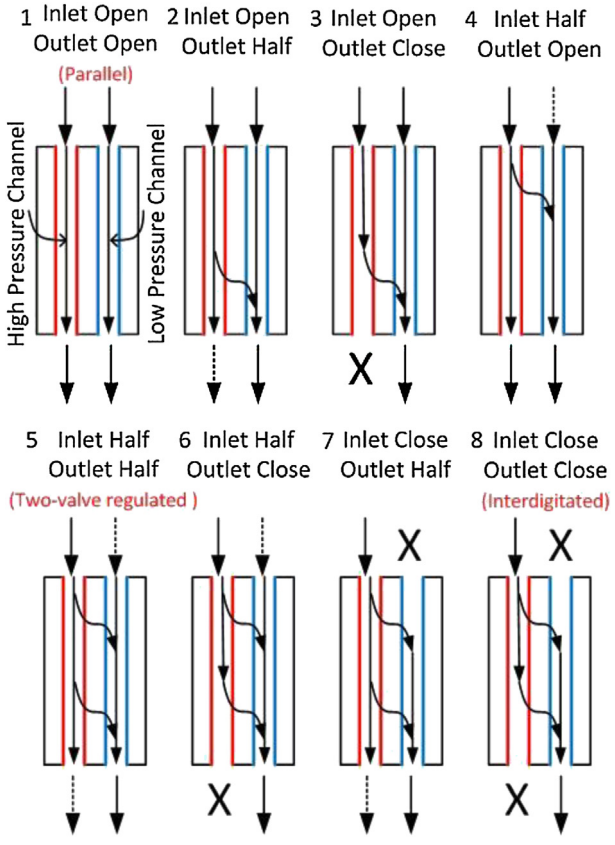


**Fig. 4.** Eight experimental flow field cases: 1 inlet valve open, outlet valve open; 2 inlet valve open, outlet valve half open; 3 inlet valve open, outlet valve closed; 4 inlet valve half open, outlet valve open; 5 inlet valve half open, outlet valve half open; 6 inlet valve half open, outlet valve closed; 7 inlet valve closed outlet valve half open; 8 inlet valve closed, outlet valve closed (HPC is shown in red and LPC is shown in s blue; solid arrow indicates the inlet/outlet is fully open, dashed arrow indicates half open, cross indicates closed) (For interpretation of the references to colour in this figure legend, the reader is referred to the web version of this article.)

### 2.4. Polarization curve test procedure

Prior to each test case, each valve was adjusted to the desired flow field configuration. Inlet valve half open was achieved using following procedure: 1) open all the valves (the cell is now at parallel flow field configuration); 2) close the inlet valve and pumping the gas at 2 sl $min^{-1}$; 3) take readings of pressure gauge 1 and pressure gauge 2, calculate the pressure difference across the inlet valve using $dP = P_1 - P_2$; 4) generally open the valve until the pressure difference drops to $dP/2$, mark this position as inlet valve half open. This manner ensures that pressure drop across the half open valve is half of the fully closed valve. Similar approach was applied to find the outlet valve half open position. The test order of eight cases was randomly picked in avoiding of biased results.

Each flow field case was then tested using a polarization curve test schedule. The fuel cell was warmed up and maintained at 80 °C prior to the experiment. The gas was pumped at temperature of 80 °C and 100% humidity. The fuel cell was run at the stoichiometry of 4 for air on the cathode and stoichiometry of 1.5 for hydrogen on the anode during the test. At the beginning of each test case, the Arbin FCTS applied 30 s of $N_2$ purging to remove water in the channels from the previous test case, and followed by 500 mA loads on the fuel cell for 1 min to warm the cell. Then it applied constant current load steps on the fuel cell starting from 0 A with increment of 3 A every step until the voltage reaches its limit. Each step lasted 30 s for the cell to reach steady state. The voltages of the last 5 s at the end of each step were averaged as cell output voltage. Readings of cell pumping pressure $P_{cell}$ (pressure gauge 1), LPCs inlet pressure $P_{(LPC,inlet)}$ (pressure gauge 2), HPCs outlet pressure $P_{(HPC,inlet)}$ (pressure gauge 3) were logged manually at every step. Average pressure difference between HPCs and LPCs was estimated using following equation:

$$\Delta P = \left(P_{(HPC,inlet)} + P_{(HPC,outlet)} - P_{(LPC,inlet)} - P_{(LPC,outlet)}\right)/2 \quad (1)$$

Where $P_{(HPC,inlet)} = P_{cell}$ is the HPCs inlet pressure, $P_{(HPC,outlet)} = P_{atm}$ is the LPCs outlet pressure. Note that when the fuel cell approaches low operation voltage (<0.2 V), it is hard to reach steady state, represented as values of pressure gauges and voltage measurements keep varying. Because the comparison between test cases are focused on fuel cell's preferable operation range (near peak power density point), higher uncertainty of last one or two data point of polarization curve will not affect drawing the conclusion. The net power density of each test cases were estimated by deducting the pumping power from the output power and then divide by cell's effective area. Each of the test cases has different pumping loss, which can be estimated by the following equation:

$$P_{pump} = \frac{\dot{m}_{air} C_p T}{\eta}\left(\left(\frac{P_{inlet}}{P_{atm}}\right)^{\frac{k-1}{k}} - 1\right) \quad (2)$$

where $\dot{m}_{air}$ is the mass flow rate of air, $C_p = 1.003$ J $kg^{-1}$ $k^{-1}$ is the specific heat of air, $T$ is the temperature of air (K), $\eta = 85\%$ is the estimated pump efficiency, $P_{inlet}$ is the air pressure at the inlet of the fuel cell (kPa), $P_{atm}$ is the atmospheric pressure (kPa), and $k = 1.4$ is the specific heat ratio.

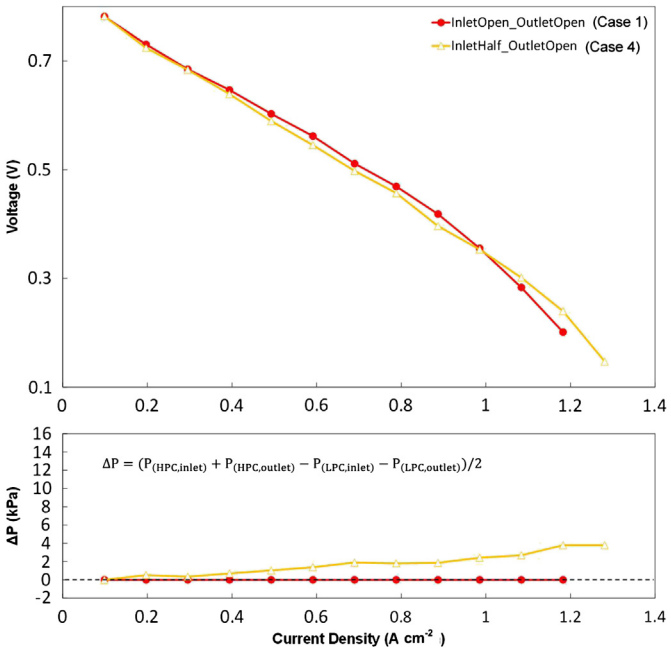


**Fig. 5.** Test results for varying inlet valve setting (Case 1, 4). Top: polarization curves; Bottom: average pressure difference between channels as a function of current density.

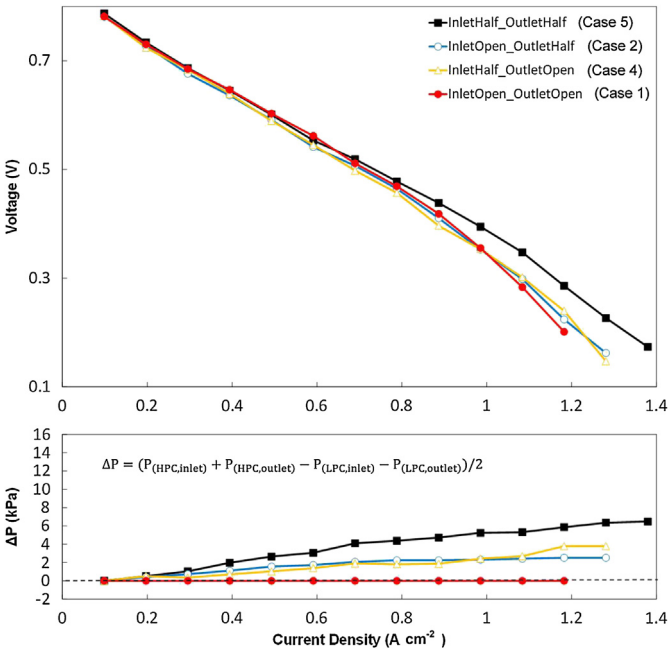


**Fig. 7.** Test results for adjusting two valves from parallel to half-half (Case 1, 2, 4, and 5). Top: polarization curves; Bottom: average pressure difference between channels as a function of current density.

## 3. Results and discussion

### 3.1. Polarization curves of one valve regulation cases

Fig. 5 compares test results of Case 1 and Case 4. LPCs inlet valves adjustment contributed to pressure difference between HPCs inlet and LPCs inlet. The average pressure difference between LPCs and HPCs of Case 4 increased with the increasing of current density. At low current density, the voltage output of Case 4 was slightly lower than Case 1. At current density of 1 A $cm^{-2}$ or higher, the voltage of Case 4 surpassed Case 1. Fig. 6 compares test results of Case 1, Case 2 and Case 3. Pressure of cell inlets was the same in these three cases. By setting HPCs outlet valve at open/half open/close positions, the channels possessed, respectively, zero/medium/high pressure differences at outlets. Polarization curves indicate that at low current density (<0.9 A $cm^{-2}$) the fuel cell output voltages of three cases were about the same. At high current

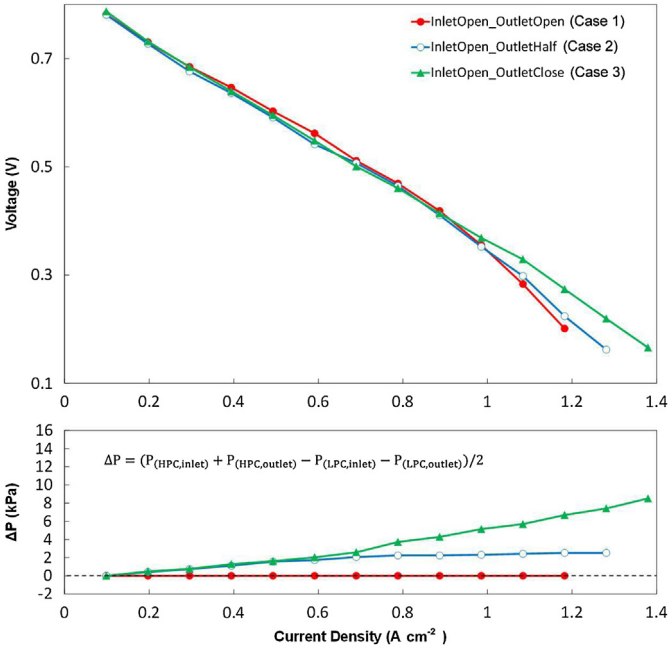


**Fig. 6.** Test results for varying outlet valve settings (Case 1, 2, 3). Top: polarization curves; Bottom: average pressure difference between channels as a function of current density.

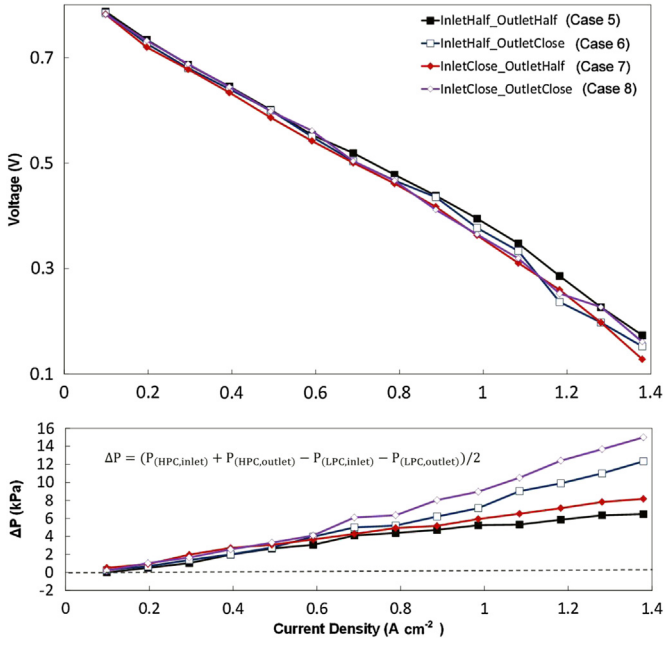


**Fig. 8.** Test results for adjusting two valves from half-half to interdigitated (Case 5–8). Top: polarization curves; Bottom: average pressure difference between channels as a function of current density.

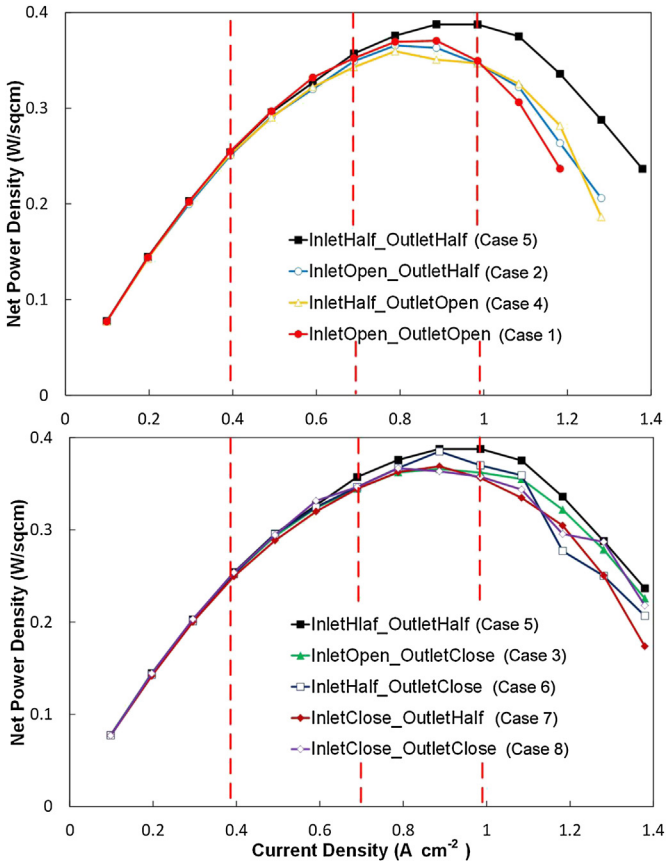


**Fig. 9.** Net power density as a function of current density for various two-valve settings. Top: parallel, open-half, half-open, half-half flow fields (Case 1,2,4,5); Bottom: half-half, open-closed, half-closed, closed-half, closed-closed flow fields (Case 3, 5–8).

density (>1 A cm$^{-2}$), Voltage output of Case 3 was higher than Case 2, and was followed by Case 1 (Case 3 > Case 2 > Case 1). Figs. 5 and 6 show adjusting inlet/outlet valves were effective in introducing pressure difference between the HPCs and the LPCs. Additionally, by only adjusting one valve, cell performances of Case 1 & Case 2 surpassed parallel flow field at current density higher than 1 A cm$^{-2}$. However this performance enhancement is not meaningful in most application because same output power is achievable at lower current density.

### 3.2. Polarization curves of two valve regulation cases

Fig. 7 compares the test results of Case 1, Case 2, Case 4 and Case 5. It showed, by adjusting both valves to half open, the resulting average pressure differences of Case 5 were approximately the sum of pressure differences of Case 2 and Case 4. At low current density, four test cases had very close voltage output. At current density of 0.7 A cm$^{-2}$ or higher, case with higher pressure difference had the higher voltage output (Case 5 > Case 2–4 > Case 1). These results indicate that under circumstances of not blocking any of the fuel cell channels, when the pressure difference between HPCs and LPCs was higher, the fuel cell had more induced cross flow contributing performance. Fig. 8 compares the test results of Case 5, Case 6, Case 7 and Case 8. The other three cases had much higher average pressure differences than the Case 5, but their polarization curve didn't showed better performance as pressure difference increases like observed in Fig. 7. By fully closing the valve(s), the fuel cell obtained highest pressure difference across the land areas. However, performance decreasing was observed associated with increasing water concentration at the area of inlet/outlet that been closed. Since cell performance of parallel flow field can be enhanced by applying back pressure to the cell, the tests presented cannot differentiate the effect of back pressure and cross flow. However, from Case 1 to Case 8, the average back pressure generally increases, and the cell performance increased from Case 1 to Case 5 but decreased from Case 5 to Case 8. It validates that in these set of tests, fuel cell performance variation was not dominated by back pressure. Having both parallel flow and cross flow (parallel interdigitated hybrid) is the major advantage of Case 5 compared to the rest of the cases. In summary, The Case 5 provided a good trade-off between promoting induced cross flow and maintaining good water removal at downstream of HPCs. As a result, Case 5 obtained the best overall performance.

### 3.3. Net power density

Fig. 9 plots the net power density against current density of eight test cases. For most of the cases, the net power density peaks were around current density of 0.8–1 A cm$^{-2}$. Test data at 0.39/0.69/0.99 A cm$^{-2}$ current density (three dashed line in Fig. 9) was

**Table 1**
Net power density comparison of 8 flow-field cases at current densities of 0.39, 0.69, 0.99 A cm$^{-2}$ and stoichiometry of 4 on the cathode.

| Inlet valve setting | Open | Open | Open | Half | Half | Half | Closed | Closed |
|---|---|---|---|---|---|---|---|---|
| Outlet valve setting | Open | Half | Closed | Open | Half | Closed | Half | Closed |
| Current density (A cm$^{-2}$) | 0.39 | | | | | | | |
| HPCs–LPCs pressure difference (kPa) | 0 | 1.103 | 1.276 | 0.689 | 1.965 | 1.999 | 2.723 | 2.551 |
| Compressor power (W) | 0.0022 | 0.0049 | 0.0050 | 0.0039 | 0.0058 | 0.0057 | 0.0068 | 0.0069 |
| Average output power (W) | 7.761 | 7.635 | 7.677 | 7.670 | 7.742 | 7.682 | 7.603 | 7.731 |
| Net power density (W cm$^{-2}$) | 0.255 | 0.251 | 0.252 | 0.252 | 0.254 | 0.252 | 0.249 | 0.254 |
| **Change in NetPowerDensity from parallel** | **0%** | **−1.57%** | **−1.18%** | **−1.18%** | **−0.39%** | **−1.18%** | **−2.35%** | **−0.39%** |
| Current density (A cm$^{-2}$) | 0.69 | | | | | | | |
| HPCs–LPCs pressure difference (kPa) | 0 | 2.068 | 2.586 | 1.896 | 4.102 | 4.999 | 4.275 | 6.102 |
| Compressor power (W) | 0.0077 | 0.0152 | 0.0193 | 0.0152 | 0.022 | 0.0241 | 0.0217 | 0.0268 |
| Average output power (W) | 10.737 | 10.647 | 10.513 | 10.454 | 10.898 | 10.571 | 10.507 | 10.577 |
| Net power density (W cm$^{-2}$) | 0.352 | 0.349 | 0.345 | 0.343 | 0.357 | 0.346 | 0.344 | 0.346 |
| **Change in NetPowerDensity from parallel** | **0%** | **−0.9%** | **−2.0%** | **−2.6%** | **1.4%** | **−1.7%** | **−2.3%** | **−1.7%** |
| Current density (A cm$^{-2}$) | 0.99 (peak power) | | | | | | | |
| HPCs–LPCs pressure difference (kPa) | 0 | 2.310 | 5.137 | 2.413 | 5.240 | 7.136 | 5.929 | 8.963 |
| Compressor power (W) | 0.0205 | 0.0287 | 0.0436 | 0.0333 | 0.043 | 0.0503 | 0.0447 | 0.0569 |
| Averaged output power (W) | 10.662 | 10.580 | 11.066 | 10.597 | 11.842 | 11.310 | 10.888 | 10.942 |
| Net power density (W cm$^{-2}$) | 0.349 | 0.347 | 0.362 | 0.347 | 0.387 | 0.370 | 0.356 | 0.357 |
| **Change in NetPowerDensity from parallel** | **0%** | **−0.6%** | **3.7%** | **−0.57%** | **10.9%** | **6.0%** | **2.0%** | **2.3%** |

extracted and listed in Table 1 for comparison. It shows that at current density of 0.39 A $cm^{-2}$, at high operation potential point, all the test cases had similar power density with differences less than 2.5%. Case 1 had the highest power density. At a current density of 0.69 A $cm^{-2}$, all the test cases still had similar power density. Case 5 had the highest power density of 0.357 W $cm^2$. At a current density of 0.99 A $cm^{-2}$, which was the peak power point of the test Case 5, Case 5 maintained the highest power density of 0.387 W $cm^{-2}$, which was 10.9% higher than Case 1, and 8.4% higher than Case 8. After taking pumping losses into account, Case 5 inherently achieved the best performance in net power density.

## 4. Conclusions

This study tested a flow field with dual manifolds capable of regulating channel pressure independently. Using two external valves, the fuel cell simulated eight different pressure configurations, including conventional parallel configuration, interdigitated flow filed configuration, and parallel configurations with inter-channel cross over. A trend of increasing fuel cell performance with the increasing of pressure difference between adjacent channels was observed. It shows higher and more uniform distributed pressure difference leads to enhanced cross flow, which improves PEMFCs' overall performance. Additionally, decrease of fuel cell performance was observed when inlet/outlet valves were closed in order to further increase pressure differences between adjacent channels. It indicates blocking channel inlets/outlets leads to high local water concentration which restricts cell performance.

In the comparative tests, the proposed two-valve regulation parallel flow field design presented the best performance due to the fact that it implements two valves/manifolds to realize gas feeding of different pressures in parallel channels as well as prevent any flow channels from being blocked. This design was observed to exceed the performance of both parallel flow field and interdigitated flow field at operation current density of 0.7 A $cm^{-2}$ or higher. The pumping loss is 0.36% of the power output. At the stoichiometry of 4 on the cathode, the proposed design achieved net performance enhancement of 10.9% compared to parallel flow field at peak power density (0.387 W $cm^{-2}$ at current density of 0.99 A $cm^{-2}$). Next step of this research is to investigate the effect of this proposed flow field on a stack level of PEMFC. Also, conducting numerical simulation of the flow field will be beneficial to examine fuel cell's local pressure gradient, cross flow, current density and water concentration.

## References

[1] X. Li, I. Sabir, J. Park, Journal of Power Sources 163 (2007) 933–942.
[2] G. Zhang, L. Guo, B. Ma, H. Liu, Journal of Power Sources 188 (2009) 213–219.
[3] X.-D. Wang, Y.-Y. Duan, W.-M. Yan, X.-F. Peng, Electrochimica Acta 53 (2008) 5334–5343.
[4] A.P. Manso, F.F. Marzo, J. Barranco, X. Garikano, M. Garmendia Mujika, International Journal of Hydrogen Energy 37 (2012) 15256–15287.
[5] J. Scholta, G. Escher, W. Zhang, L. Küppers, L. Jörissen, W. Lehnert, Journal of Power Sources 155 (2006) 66–71.
[6] J. Park, X. Li, Journal of Power Sources 163 (2007) 853–863.
[7] J.W. Park, K. Jiao, X. Li, Applied Energy 87 (2010) 2180–2186.
[8] B. Ramos-Alvarado, A. Hernandez-Guerrero, D. Juarez-Robles, P. Li, International Journal of Hydrogen Energy 37 (2012) 436–448.
[9] J. Bachman, A. Santamaria, H.-Y. Tang, J.W. Park, Journal of Power Sources 198 (2012) 143–148.
[10] D. Spernjak, A.K. Prasad, S.G. Advani, Journal of Power Sources 195 (2010) 3553–3568.
[11] J.P. Owejan, T.A. Trabold, D.L. Jacobson, D.R. Baker, D.S. Hussey, M. Arif, International Journal of Heat and Mass Transfer 49 (2006) 4721–4731.
[12] A. Su, F.-B. Weng, C.-Y. Hsu, Y.-M. Chen, International Journal of Hydrogen Energy 31 (2006) 1031–1039.
[13] A. Higier, H. Liu, Journal of Power Sources 193 (2009) 639–648.
[14] Z. Shi, X. Wang, Journal of Power Sources 185 (2008) 985–992.
[15] P.V. Suresh, S. Jayanti, A.P. Deshpande, P. Haridoss, International Journal of Hydrogen Energy 36 (2011) 6067–6072.
[16] X.-D. Wang, Y.-Y. Duan, W.-M. Yan, X.-F. Peng, Journal of Power Sources 175 (2008) 397–407.
[17] X.-D. Wang, Y.-Y. Duan, W.-M. Yan, Journal of Power Sources 173 (2007) 210–221.
[18] J.P. Owejan, T.A. Trabold, D.L. Jacobson, M. Arif, S.G. Kandlikar, International Journal of Hydrogen Energy 32 (2007) 4489–4502.
[19] H.-Y. Tang, A. Santamaria, J.W. Park, C. Lee, W. Hwang, Journal of Power Sources 196 (2011) 9373–9381.
[20] H.-Y. Tang, A. Santamaria, J. Kurniawan, J.W. Park, T.-H. Yang, Y.-J. Sohn, Journal of Power Sources 195 (2010) 6774–6781.
[21] A. Higier, H. Liu, International Journal of Hydrogen Energy 35 (2010) 2144–2150.
[22] A. Santamaria, H.-Y. Tang, J.W. Park, G.-G. Park, Y.-J. Sohn, International Journal of Hydrogen Energy 37 (2012) 10836–10843.
[23] T.V. Reshetenko, G. Bender, K. Bethune, R. Rocheleau, Electrochimica Acta 56 (2011) 8700–8710.
[24] X. Li, I. Sabir, International Journal of Hydrogen Energy 30 (2005) 359–371.